



# MEASUREMENT OF INCLUSIVE DOUBLE-DIFFERENTIAL $N_{\mu}$ CHARGED-CURRENT CROSS SECTION WITH IMPROVED ACCEPTANCE IN THE T2K OFF-AXIS NEAR DETECTOR

N.Renuka, K. Ashok Kumar, VIJAYA BELGAL ANILA

Assistant Professor,

Department of H&S (Physics)

Ellenki College of Engineering & Technology

Hyderabad

## I. INTRODUCTION

T2K is an experiment located in Japan with the primary aim of studying neutrino oscillations [1]. It was designed to measure with high precision the  $\nu_{\mu} \nu_{\mu}$  disappearance channel and to discover the  $\nu_{\mu} \nu_{e}$  appearance channel.

In addition to the oscillation measurements, T2K has an ongoing program to study neutrino interactions using the near detector complex in order to improve the understanding and modeling of these interactions. Results from this program, as exemplified by those presented in this paper, are interesting in their own right and can be used to constrain and reduce the systematic errors arising from cross section uncertainties in the extraction of neutrino oscillation parameters. Inclusive measurements provide a clear signals which are very valuable to test different models.

Previously, T2K reported the measurement of the flux-integrated double differential cross section for muon neutrino charged-current interactions on carbon [2]. Since that time, many improvements have been made in the analysis. The results presented in this paper were obtained with more data, reduced neutrino flux uncertainties (thanks to new NA61/SHINE measurements [3]), increased angular acceptance, reduced background contamination and a different unfolding method. All the improvements are described in more detail below.

The paper is organized as follows: we first summarize the experimental setup in Sec. II, which contains the description of the off-axis beam, the near detector and the neutrino event

generators used in the present analysis. The selection of the muon neutrino interaction samples is presented in Sec. III together with the summary of the detector systematic uncertainties. The analysis method is explained in Sec. IV and the results are given in Sec. V.

## II. EXPERIMENTAL APPARATUS

### A. T2K beamline and flux prediction

The neutrino beam used by T2K is produced at the J-PARC Laboratory in Tokai, Japan. In this process, 30 GeV/c protons are extracted from the main ring accelerator at J-PARC onto a graphite target, producing secondary particles consisting primarily of pions and kaons.

‡ affiliated member at Kavli IPMU (WPI), the University of Tokyo, Japan

§ also at National Research Nuclear University "MEPhI" and Moscow Institute of Physics and Technology, Moscow, Russia

fj also at JINR, Dubna, Russia

\*\* also at Institute of Particle Physics, Canada

†† also at BMCC/CUNY, Science Department, New York, New York, U.S.A.

The hadrons exiting the target are focused by three magnetic horns and allowed to decay in a decay volume. The decaying hadrons produce neutrinos (primarily of muon flavor) that continue to the near and far detectors while the other particles range out. Depending on the polarity of the electric current in the horns, a beam composed of mostly neutrinos ( $\nu$ -mode) or antineutrinos ( $\bar{\nu}$ -mode) and with

energy peaked at 0.6 GeV is produced. The T2K beamline hardware has been described in detail elsewhere [1].

The simulation that is used to predict the neutrino flux and its associated uncertainty is described in detail in [4]. The uncertainties are dominated by the hadron production model and, to second order, by the beamline configuration. Currently, the uncertainty on the  $\nu_\mu$  beam flux at the near detector varies from 10% to 15% depending on the neutrino energy. The error associated with the flux in the results presented here has been reduced with respect to that used in the previous analysis [2], in part, because the model of hadron production from the target is tuned using the full 2009 thin-target dataset by the NA61/SHINE experiment [3]. The previous analysis used the 2007 dataset [5].

#### B. The off-axis near detector

The off-axis near detector (ND280) is made-up of two main components, the  $\pi 0$  detector (POD [6]) and the Tracker region. Both parts are contained in a metal basket box surrounded by electromagnetic calorimeters (ECal [7]) and a warm dipole magnet. The magnet provides a 0.2 T field allowing for momentum measurement and charge separation. Outside the ECal and magnet coil is the magnet flux return yoke and the side muon range detector (SMRD [8]).

The Tracker region contains two fine-grained detectors (FGDs [9]) sandwiched between three gas time projection chambers (TPCs [10]). The TPCs contain a drift gas mixture which is ionized when a charged particle crosses it. The TPCs provide excellent track and momentum reconstruction. The observed energy loss in the TPCs, combined with the measurement of the momentum, is used for particle identification.

The most upstream FGD (FGD1) consists of polystyrene scintillator bars, which are oriented vertically and horizontally and perpendicular to the beam direction. FGD1 is comprised of carbon (86.1%), hydrogen (7.4%) and oxygen (3.7%), where the percentages represent the mass fraction of each element. The most downstream FGD (FGD2)

is similar to FGD1 except that the scintillator layers are interleaved with water layers. FGD1 is the active target in this analysis. The fiducial volume (FV) begins 58 mm inward from the lateral edges as shown in Fig. 1.

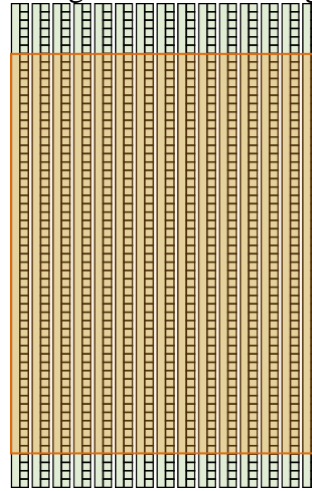


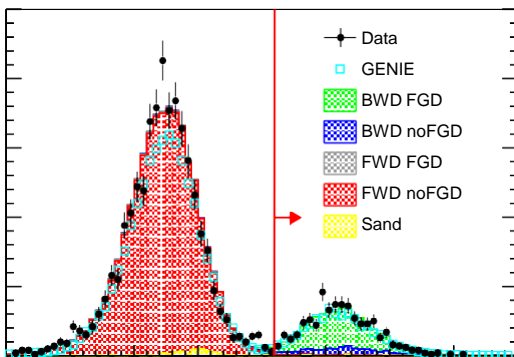
FIG. 1. Schematic view of FGD1. The orange region indicates the fiducial volume.

interactions happening upstream of the active target.

The SMRD consists of 440 scintillator modules inserted in the air gaps between sections of the magnet flux return yoke. Horizontal (vertical) modules are composed of four (five) plastic scintillation counters. In this analysis, the SMRD is used to identify and measure the range of muons at high angles with respect to the beam direction. The range provides information about the muon momentum.

The ECal consists of 13 modules surrounding the inner detectors. The tracker module is covered by six modules in the sides (BarrelECal) and one module downstream (DsECal). The modules are made up of plastic scintillator bars interleaved with lead sheets. In this analysis, the ECal is used to complement the reconstruction of the inner detectors. As with the SMRD, it is used to measure the range/momentum of muons escaping, from inner detectors, at high angles with respect to the beam direction. In addition, electromagnetic showers and minimally ionizing tracks passing through the ECal can be identified using a multivariate analysis quantity RMIP/EM determined by the features of the reconstructed clusters in the ECal [11].

In this analysis, the timing information for particles crossing the different detectors of ND280 is used for the first time. When a particle crosses a detector composed by scintillators, the time information from each individual hit is corrected for the light propagation time inside the fibers and for the time offset of each slave clock module [1]. Then, the corrected time and position of the hits are used to define an average time ( $T$ ). Finally, the time of flight (ToF) variable ( $ToF = \frac{TX - TY}{c}$ ) between two detectors X and Y is constructed. This information FIG. 2. ToF between FGD1-BarrelECal for tracks crossing BarrelECal-TPC1-FGD1. Stacked histograms indicate the prediction from NEUT of the true direction and whether the true start position is inside FGD1. Data distributions show their statistical error bars. The region indicated by the red arrow shows tracks that are reconstructed as backward-going. They are chosen that give the lowest wrong used to determine the direction of tracks crossing the following pairs of detectors: FGD1-FGD2, FGD1-POD, and FGD1-BarrelECal (see Fig. 2).



### C. Event generators

Two event generators, NEUT 5.3.2 [12] and GENIE

[13], are used to simulate the interaction of neutrinos in the near detector and the effect of the nuclear medium on the produced particles. The modeling of the main interaction channels and their associated uncertainties is described below.

### 1. Charged-current interactions without pion production

Charged-current (CC) interactions without pion production are referred to here as charged-current quasi-elastic-like, or CCQE-like, interactions. The sample of such interactions is composed mainly of CCQE reactions. However, nuclear effects can cause other processes to be included in this category.

For the CCQE channel, the primary neutrino-nucleon interaction is modeled in a similar fashion by both generators. Each uses an implementation of the Llewellyn-Smith formalism [14] through Lorentz-invariant form factors (FFs). Both generators relate the vector FF to the electromagnetic FFs, for which the parametrization BBA2005 is used [15]. For the axial FF, a dipole shape with  $g_A = 1.267$  is used in both generators. However, the default axial mass parameter,  $M_A$ , used in each generator differs. In NEUT,  $M_A = 1.21 \text{ GeV}/c^2$ , while in GENIE,  $M_A = 0.99 \text{ GeV}/c^2$ . Finally, they use the same pseudo-scalar FF suggested by the partially conserved axial current (PCAC) hypothesis.

The majority of the CCQE interactions take place on bound nucleons. The nuclear model differs between the two generators. In the case of GENIE, the Bodek-Richie version of the Relativistic Fermi Gas (RFG) model is used, which incorporates short range nucleon-nucleon correlations [16]. For NEUT, a different nuclear model is used based on the spectral functions from [17]. Moreover, NEUT includes the multi-nucleon interaction (2p2h) model from Nieves et al. [18], as it is thought that interactions on more than one bound nucleon contribute significant strength to the signal relative to the single particle CCQE interaction. Pauli blocking is implemented equally in both generators (reject events with the momentum of the outgoing nucleon below the Fermi momentum of the nucleus).

The CCQE and 2p2h interactions are parametrized in NEUT with several target-dependent parameters (subscripts “C” and “O” represent parameters for carbon and oxygen targets, respectively): the quasielastic

axial mass ( $M_A = 1.21 \pm 0.3 \text{ GeV}/c^2$ ), the binding energy ( $E_C = 25 \pm 25 \text{ MeV}$  and  $E_O = 27 \pm 27 \text{ MeV}$ ), the Fermi momentum ( $p_C = 217 \pm 30 \text{ MeV}/c$  and  $p_O = 225 \pm 30 \text{ MeV}/c$ ) and the 2p2h cross-section normalization ( $MECC = 1 \pm 1$  and  $MECO = 1 \pm 1$ ). The nominal values for these parameters and the associated uncertainties were chosen based on a study of the MINERvA and MiniBooNE datasets [19]. Large uncertainties without correlations were assigned in order to cover the tensions between the two datasets and different nuclear models.

## 2. CC interactions with pion production

Pion production is treated differently in the two event generators. NEUT generates interactions with single pion production using a resonant model when  $W < 2 \text{ GeV}/c^2$ . Single pion production above that value and the rest of pion production channels are generated with a DIS model. In contrast, GENIE does not restrict the resonant model to the single pion decay channel. This model is switched off when  $W > 1.7 \text{ GeV}/c^2$  (to avoid double counting with its DIS model). Below that value, the normalization of the single pion and two pions production channels from its DIS model are tuned.

Resonant pion production is based on the Rein-Sehgal model for both generators [20]. In NEUT, the model uses 18 resonances taking into account their interferences. The default parameters for the FFs are taken from [21]. In contrast, GENIE incorporates 16 resonances without including interference terms and the default FFs are taken from [22].

The resonant model has three parameters in NEUT: the resonant axial mass ( $M_{RES} = 0.95 \pm 0.15 \text{ GeV}/c^2$ ), the normalization of the axial form factor for resonant pion production ( $C_A = 1.01 \pm 0.12$ ) and the normaliza-

tion of the isospin non-resonant component predicted in the Rein-Sehgal model ( $I_{1/2} = 1.3 \pm 0.2$ ). Their nominal values and associated uncertainties, with no correlation assumed, were obtained by comparison with available

low energy neutrino-deuteron single pion production data [23].

Both NEUT and GENIE model deep inelastic scattering using the same GRV98 PDF parametrization [24] including a Bodek-Yang correction to describe scattering at low  $Q^2$ . The Bodek-Yang correction differs slightly between the two generators, as NEUT uses [25] and GENIE uses [26]. An energy dependent normalisation uncertainty (10% at 4 GeV) is used based on MINOS CC-inclusive data [27].

For coherent reactions, both generators use the Rein-Sehgal model [28] including a correction that takes into account the lepton mass [29]. However, the implementation of the model differs slightly. NEUT follows the prescriptions and data fit of pion scattering from [28], leading to different cross sections for low momentum pions. The MINERvA experiment has reported results which are consistent with coherent pion production at energies around 1 GeV [30]. Considering that result, a 30% normalization uncertainty in CC coherent interactions is included.

## 3. Neutral-current interactions

Neutral-current (NC) interactions affect the background prediction in this analysis. Therefore, an NC normalization parameter was included that scales elastic, resonant kaon and eta production, and DIS events. A 30% uncertainty is assigned for those channels, motivated by poor constraints from external data.

## 4. Hadronization and final state interactions

Hadron production and transport inside the nuclear medium are also simulated by the event generators. In this analysis, the prediction of these processes is particularly important for pions, as they contribute the main background.

The hadronization model (or fragmentation model) determines the kinematics of the primary outgoing hadrons, prior to final state

interactions (FSI), given a particular interaction. In the high invariant mass region ( $W_{NEUT} > 2 \text{ GeV}/c^2$  and  $W_{GENIE} > 3 \text{ GeV}/c^2$ ), the hadronization is simulated using the PYTHIA5 and PYTHIA6 predictions [31] in NEUT and GENIE, respectively. These predictions are unsatisfactory near the pion production threshold. So, both generators include a different phenomenological description based on Koba-Nielsen-Olesen (KNO) scaling [32] in the low invariant mass region. Moreover, the transition between the two regions is handled differently between the two generators. Specifically, GENIE includes the AGKY model [33] for  $W < 3 \text{ GeV}/c^2$  and the transition region ( $2.3 \text{ GeV}/c^2 < W < 3 \text{ GeV}/c^2$ ) in which the PYTHIA model is turned on gradually.

In GENIE, several parameters affect pion kinematics. In particular, for single pion states four parameters are notable: the nucleon  $x_F$  ( $p_2$ ), PDFs for  $N\pi$  hadronic states, the nuclear formation zone, and the pion angular distribution in  $\Delta$  resonant pion production. Their nominal values and associated uncertainties are estimated based on recommendations from the GENIE Collaboration [13]. These parameters are treated as uncorrelated. Near an energy of 1 GeV, pions immersed in a highly dense nuclear medium are very likely to interact. Both generators simulate pion FSI using the intra-nuclear cascade approach, though they use different predictions for the interaction probabilities. In the case of NEUT, pion interaction probabilities are dependent on the momentum of the pion: if  $p_\pi < 500 \text{ MeV}/c$ , NEUT uses a density dependent model [34] and if  $p_\pi > 500 \text{ MeV}/c$  the probabilities are extracted from pion-nuclear scattering experiments [35]. GENIE uses a model called INTRANUKE hA which extracts the interaction probabilities from several experiments up to 300 MeV/c, while for higher energies it is based on the CEM03 predictions [36]. The uncertainties associated with the pion interaction probabilities and their correlations are estimated

using the same methodology as in [37].

### III. $\nu_\mu$ CC SAMPLES

This analysis uses data collected in  $\nu$ -mode between November 2010 and May 2013. The total sample comes from 5.7 1020 protons on target (POT), which is a factor of five larger than that used in the similar previously published analysis from T2K [2].

Simulated Monte Carlo (MC) interactions within the ND280 subdetectors and magnet were generated using both NEUT and GENIE. The background interactions in the materials surrounding ND280, so-called sand interactions, were generated using NEUT. Both interactions in ND280 and in the surrounding material were generated using the same neutrino beam simulation, detector simulation and reconstruction.

In this analysis, events containing muons emanating from interactions that occur in the fiducial volume (FV) of FGD1 are selected. These events are candidate  $\nu_\mu$  CC interactions. The events within this sample that are true  $\nu_\mu$  CC events belong to the category referred to here as  $\nu_\mu\text{CC-}\mu$ .

Background events in the initial selection include: interactions not happening in the FV (either inside or outside the magnet volume, referred to as ‘out FV’ and ‘sand  $\mu$ ’, respectively); interactions happening in the FV but not actually a  $\nu_\mu$  CC event, referred to as  $\text{no}\nu_\mu\text{CC}$ ; or being  $\nu_\mu$  CC but where the muon candidate track is not the outgoing muon, herein called  $\nu_\mu\text{CC-no}\mu$ .

The cross-section results presented here are based on

the kinematics of the outgoing muon. Specifically, the results are given as a function of the muon momentum,  $p_\mu$ , and the cosine of the muon emission angle with respect to the neutrino direction,  $\cos \theta_\mu$ . The event selection criteria and performance, as well as the systematic uncertainties associated with the detector response are described below.

#### A. Event selection

In previous T2K work on this topic, the analysis was optimized to select forward-going muons originating from FGD1 and making a long track (at least 19 clusters as described in section III A 1) through TPC2, which is downstream of FGD1 [2]. The current work aims to include the so-called high-angle tracks which miss or barely cross the TPCs, as well as long backward-going tracks in TPC1 (upstream of FGD1). The addition of backward-going muon candidates in the event selection is possible only with the introduction of timing information correlated between subdetectors.

In this analysis, events are broken into samples according to the muon direction. If the muon candidate in the event goes forward (in the direction downstream of FGD1 into TPC2), the event is part of the forward (FWD) sample. If the muon goes backward (in a direction upstream of FGD1 into TPC1), the event is part of the backward (BWD) sample. Similarly, if the muon candidate in the event is at a high angle in the forward or backward direction, the event is categorized as high-angle forward (HAFWD) or high-angle backward (HABWD), respectively. In the FWD/BWD selections, the muon candidate must have long TPC segments, while tracks with short or no TPC segment are used in the HAFWD/HABWD (see Fig. 3).

For events to be considered in this analysis, they must occur within the time window of one of the 8 beam bunches per  $5 \mu\text{s}$  spill RF structure of the beam. The full spill is required to be of good quality. Events are resolved in time by bunch and then processed. Given the beam intensity for these runs, the frequency of multiple neutrino interactions happening in the same beam spill (so-called pile-up events) is very low. This is ignored in the sample selection and included in the systematic error treatment.

In order to avoid having multiple muon candidates, the analysis looks for candidates sequentially in the different event selections. The ordering for this process is FWD, BWD, and then the high angle categories. FWD and BWD have a higher priority than the high angle categories because the muon PID from the TPCs is more accurate than in the ECals. The

FWD(HAFWD) selection has a higher priority than the BWD(HABWD) because forward-going muon happen much more often than backward-going ones.

Additionally, two control regions are selected to constrain neutral current event rates and pion final state

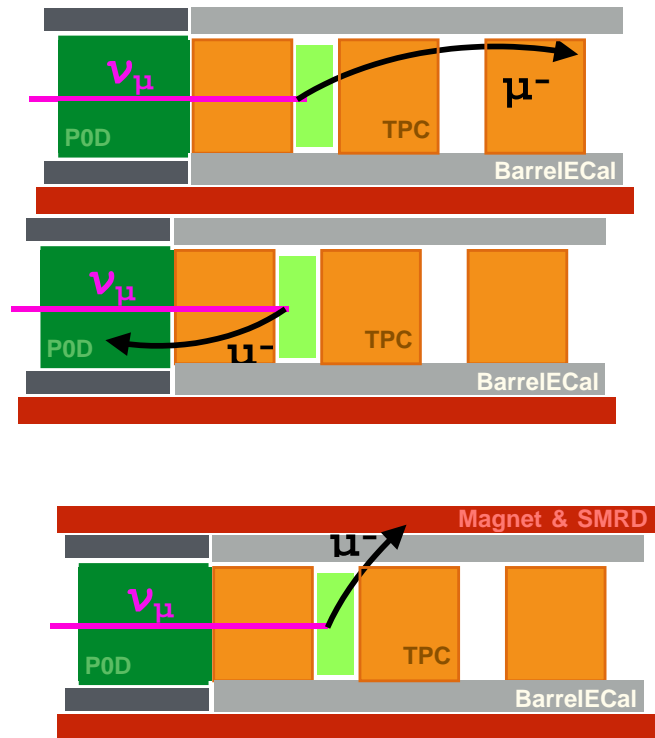


FIG. 3. Schematic representation of the regions of interest for each selection.

interactions. The control regions are non-signal regions of phase space close enough to the signal region that the backgrounds are similar to that in the signal region. The backgrounds used in the model are tuned using the data observed in the control regions. The control region selection is described in section III A 4.

#### 1. Forward selection

The selection criteria for the FWD sample are very similar to those used previously, though some further optimization has been performed. The cuts used to extract the FWD sample are described below.

**Quality and FV:** This selection considers negatively charged tracks originating in the FGD1 FV which have TPC track segments containing more than 18 clustered hits in the TPC. If multiple tracks satisfy these criteria, the muon candidate is the one with highest momentum and going forward (by timing). In order to reduce the contamination from events occurring outside the FV, tracks starting in the most upstream layer of FGD1 are rejected.

**Muon PID:** This cut is applied to the muon candidate using discriminator functions calculated for muon, pion and proton hypotheses based on the energy loss and momentum measurement of the TPC. These functions are the same as used in the previous analysis [2]. This cut rejects protons, pions and low momentum electrons (below 500 MeV/c). Moreover, two new PID cuts below have been developed in order to reduce the pion contamination of this sample (which is the main background in this analysis).

– **Muon FGD2 PID:** High energy pions are more likely to stop in FGD2 than muons. Therefore, it is required that the muon candidate leave the FGD2 active volume with a momentum above 280 MeV/c. This is expected to reduce the pion contamination by 15% while leading to a loss of 0.3% of the muons.

– **Muon ECal PID:** For tracks entering the BarrelECal or DsECal modules, the multivariate analysis quantity RMIP/EM (based on the features of the reconstructed clusters in the ECal [11]) is used. These tracks must have RMIP/EM < 15, which is estimated to reduce the pion contamination by 7% while removing 0.3% of the muons.

**Veto:** One of the main backgrounds in this analysis are interactions happening outside the FV. This contamination can be reduced further by using the two cuts described below:

– **Upstream background veto:** Due to reconstruction failures and multiple scattering, a reconstructed track can be broken into two unmatched segments. One of those

can have its beginning in the FV, mimicking an interaction that originates in the FV. In the previous analysis, such events were rejected if the second highest momentum track started more than 150 mm upstream of the muon candidate. This cut was found to be too restrictive because it removed events with a forward going muon and a second particle going backward. In the current analysis, the ratio between the momentum of the muon candidate and the other track is used. Ideally, if the muon candidate is a broken track, this ratio should be bigger than one since the first segment of the track has a higher momentum than the second segment. Therefore, the distance between both tracks, or segments, as well as their momentum ratio are used. Cut values are chosen that give the highest purity times efficiency.

– **Broken track cut :** This cut rejects events where the reconstruction procedure mistakenly breaks a single track into two tracks

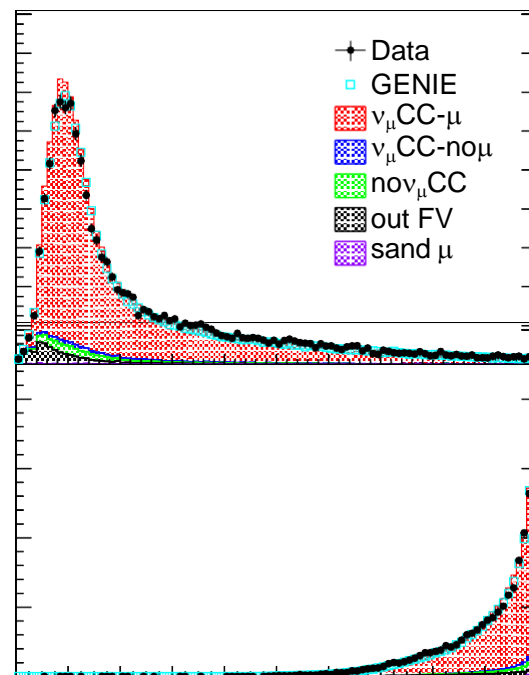


FIG. 4. Momentum (top) and cosine of emission angle (bottom) for the muon candidate when all selection criteria are fulfilled in the FWD selection. Stacked histograms indicate different reaction types predictions from NEUT. Empty rectangles indicate the prediction from GENIE. Data distributions show their statistical error bars.

where the first is a FGD1 segment and the second is reconstructed to begin in the last layers of FGD1 and goes through the downstream TPC module. In this mis-reconstruction pathology, the second track is considered a muon candidate. For such events, the start position of muon candidate track is within the two most downstream layers of FGD1. The broken track cut rejects these events by requiring that there be no reconstructed track with only a FGD1 segment when the start position of the muon candidate is in one of the last two layers of FGD1.

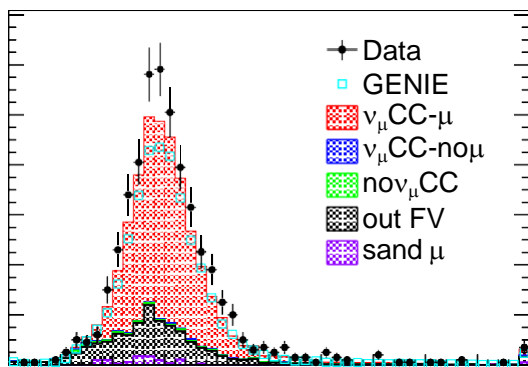


Fig. 4 shows the reconstructed kinematics for muon candidates in the FWD sample in the data together with the prediction from NEUT and GENIE.

### 3. High Angle selection

In the selection for the high angle samples (HAFWD and HABWD), the muon candidates are mostly (or all) contained in the FGD1, ECal and SMRD subdetectors. A detailed explanation of the selection criteria is shown below.

**Quality and FV:** High angle tracks starting in FGD1 FV and stopping either in SMRD or BarreIECal are considered. The stopping requirement is needed in order to compute the momentum of the track by range. The contamination from events occurring outside the FV is reduced by rejecting tracks starting in the most upstream or downstream layers of FGD1.

**Muon PID:** The TPC PID information is not reliable for high angle tracks since they have no (or short) TPC segments. The SMRD and BarreIECal information forms the basis of the high angle track PID. Tracks that reach the SMRD in the HAFWD sample are good muon candidates (1200 tracks). In the HABWD sample, most tracks reaching the SMRD come from out of the FV. Consequently, tracks reaching the SMRD in the HABWD sample are rejected (70 tracks). Tracks not reaching the SMRD and stopping in the BarreIECal region of the detector (4250 and 1250 tracks for HAFWD and HABWD respectively) are considered as muon candidates if the multivariate analysis

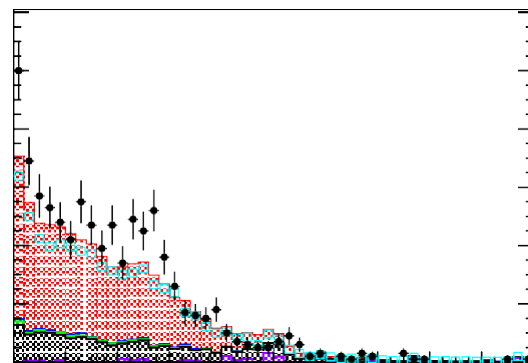


FIG. 5. Momentum (top) and cosine of emission angle (bottom) for the muon candidate when all selection criteria are fulfilled in the BWD selection. Stacked histograms indicate different reaction types predictions from NEUT. Empty rectangles indicate the prediction from GENIE. Data distributions show their statistical error bars.

quantity  $RMIP/EM < 0$ . Besides, we reduce the contamination of protons rejecting events that release high amount of energy in short distances within the BarreIECal.

**Veto:** The upstream background veto, introduced in the FWD selection, is used for the high angle samples. For this veto, the distance and momentum ratio relation was optimized for forward going and backward going candidates independently.

Fig. 6 and Fig. 7 show the reconstructed kinematics for the muon candidates in the HAFWD and HABWD samples in the data together with the prediction from NEUT and GENIE.



4. Control regions selection

As mentioned earlier, uncertainties associated with the modeling of backgrounds and pion kinematics, neutral current normalization and pion final state interactions

FIG. 6. Momentum (top) and cosine of emission angle (bottom) for the muon candidate when all selection criteria are fulfilled in the HAFWD selection. Stacked histograms indicate different reaction types predictions from NEUT. Empty rectangles indicate the prediction from GENIE. Data distributions show their statistical error bars.

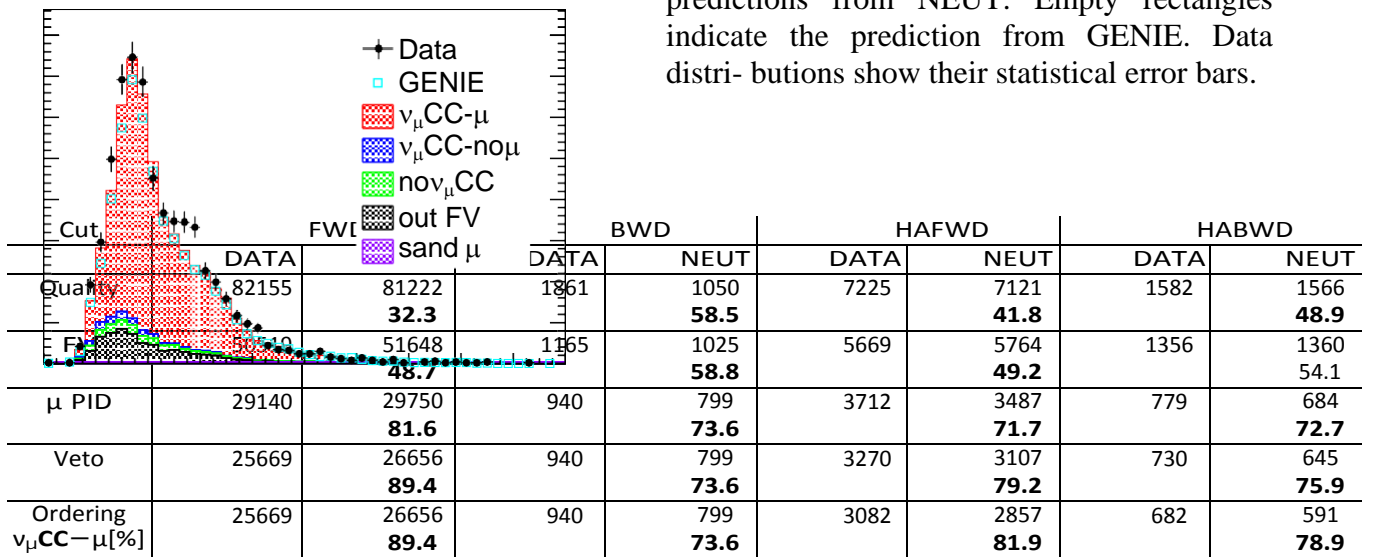


TABLE I. The selected number of events and signal purities percentage (in bold) in each sample as successive requirements are added for data and MC. The cut in last row refers to the priority order in cases where a muon candidate has been found in two samples.

RESULTS AND CONCLUSIONS

The flux-integrated total cross section is computed by data is changed depending on the source of uncertainty as described below.

To evaluate the uncertainty due to data statistics, toy experiments are produced applying a Poisson fluctuation to the number of reconstructed events in the data for each bin and sample. For each toy, the fluctuated data are unfolded using as prior the nominal MC and the cross section is computed using Eq. 1. The statistical error in each bin is taken as width of the cross section distribution for many toys.

The methodology used to estimate systematic uncertainties involves reweighting the MC prediction for each toy experiment. Parameters associated to each systematic error are thrown according to a Gaussian distribution around the

nominal value, following the prior errors and taking into account correlations. Then, for each toy, the data is unfolded using as prior the reweighted MC. In

addition,  $\Phi$ , NFV and  $\epsilon v_{\mu}CC-\mu$  are also weighted using

the thrown value of the parameters. Finally, the cross section is computed using Eq. 1 for each toy. The uncertainty in each bin is taken as width of the cross section distribution for many toys.

Fig. 12 shows a comparison of the fractional error associated to each source of uncertainty using 1500 toy models. Throughout most of the phase space, the dominant systematic uncertainty is the flux. In the backward region, the neutrino interaction modeling dominates, with the largest contribution coming from the

uncertainty assigned to the MA parameter. The detector systematic becomes relevant in the high angle region ( $0.25 < \cos \theta_{\mu} < 0.25$ ) due to the large uncertainties in FGD-ECal(SMRD) matching efficiencies, and at very low momentum where the out of FV contribution is more pronounced. The statistical uncertainty is dominant in the high momentum region where the number of reconstructed events is lower (except at low angles in the forward direction).

It is interesting to note that the systematic uncertainties associated with the signal and background modeling give a relatively unimportant contribution to the overall inclusive cross section uncertainty because of the high purity and efficiency for the signal sample. The systematic

$$\sigma_{\text{DATA FIT W/ NEUT}} = (6.950 \pm 0.049[\text{stat}] \pm 0.123[\text{syst}]$$

$$\pm 0.608[\text{flux}]) \times 10^{-39} \text{cm}^2 \text{nucleon}^{-1}$$

$$\sigma_{\text{DATA FIT W/ GENIE}} = (6.850 \pm 0.048[\text{stat}] \pm 0.121[\text{syst}]$$

$$\pm 0.599[\text{flux}]) \times 10^{-39} \text{cm}^2 \text{nucleon}^{-1}$$

This is compatible with predictions from the two event generators:  $\sigma_{\text{NEUT}} = 7.108 \times 10^{-39} \text{cm}^2 \text{nucleon}^{-1}$  and  $\sigma_{\text{GENIE}} = 6.564 \times 10^{-39} \text{cm}^2 \text{nucleon}^{-1}$ . It is known that the detector performance varies substantially as a function of the momentum and angle of the outgoing muon.

Therefore, the extracted value using the total cross section must be interpreted cautiously. This result shows good agreement with the one obtained in [2].

The flux-integrated, double-differential cross section is computed as function of the outgoing muon kinematics using the methodology described in Sec. IV A and Sec. IV B using two independent MC generators detailed in Sec. II C. Fig. 13 shows the results for the unfolded data as well as the NEUT and GENIE predictions. A small disagreement is observed in the low momentum and very forward regions when using different event generators as prior. This bias is not due to unfolding but due to the different efficiency corrections in that region of

the phase space for NEUT and GENIE as shown in Fig. 11. The muon neutrino flux used in this analysis and the measured cross section values, errors and correlation matrix can be found in [39].

This result is compared to the NEUT and GENIE predictions, showing in both cases high  $\chi^2$  values with respect to the total number of bins, 71. In the new regions of phase space (high angle and backward-going muons) there is good agreement but uncertainties are still large. For forward-going muons the binning is finer and interesting structures are observed.

#### ACKNOWLEDGEMENTS

We thank the J-PARC staff for superb accelerator performance. We thank the CERN NA61/SHINE Collaboration for providing valuable particle production data. We acknowledge the support of MEXT, Japan; NSERC (Grant No. SAPPJ-2014-00031), NRC and CFI, Canada; CEA and CNRS/IN2P3, France; DFG, Germany; INFN, Italy; National Science Centre (NCN) and Ministry of Science and Higher Education, Poland; RSF, RFBR, and MES, Russia; MINECO and ERDF funds, Spain; SNSF and SERI, Switzerland; STFC, UK; and DOE, USA. We also thank CERN for the UA1/NOMAD magnet, DESY for the HERA-B magnet mover system, NII form SINET4, the WestGrid and SciNet consortia in Compute Canada, and GridPP in the United Kingdom. In addition, participation of individual researchers and institutions has been further supported by funds from ERC (FP7), H2020 Grant No. RISE-GA644294-JENNIFER,

EU; JSPS, Japan; Royal Society, UK; the Alfred P. Sloan Foundation and the DOE Early Career program, USA

[1] K. Abe et al. (T2K Collaboration), Nucl. Instrum. Methods Phys. Res., Sect. A 659, 106 (2011).

[2] K. Abe et al. (T2K Collaboration), Phys. Rev. D 87, 092003 (2013).

[3] N. Abgrall et al. (NA61/SHINE Collaboration), Eur. Phys. J. C 76, 84 (2016).

[4] K. Abe et al. (T2K Collaboration), Phys. Rev. D 87, 012001 (2013).

- [5] N. Abgrall et al. (NA61/SHINE Collaboration), Phys. Rev. C 85, 035210 (2012).
- [6] S. Assylbekov et al., Nucl. Instrum. Methods Phys. Res., Sect. A 686, 48 (2012).
- [7] D. Allan et al., J. Instrum. 8, P10019 (2013). [8] S. Aoki et al., Nucl. Instrum. Methods Phys. Res., Sect. A 698, 135 (2013).
- [9] P. Amaudruz et al., Nucl. Instrum. Methods Phys. Res., Sect. A 696, 1 (2012).
- [10] N. Abgrall et al., Nucl. Instrum. Methods Phys. Res., Sect. A 637, 25 (2011).
- [11] K. Abe et al. (T2K Collaboration), Phys. Rev. D 89, 092003 (2014).
- [12] Y. Hayato, Acta Phys. Pol. B 40, 2477 (2009).
- [13] C. Andreopoulos et al., Nucl. Instrum. Methods Phys. Res., Sect. A 614, 87 (2010).
- [14] C. L. Smith, Phys. Rep. 3, 261 (1972).
- [15] R. Bradford et al., Nucl. Phys. B Proc. Suppl. 159, 127 (2006).
- [16] A. Bodek and J. L. Ritchie, Phys. Rev. D 23, 1070 (1981).
- [17] O. Benhar and A. Fabrocini, Phys. Rev. C 62, 034304 (2000).
- [18] J. Nieves et al., Phys. Rev. C 83, 045501 (2011).
- [19] C. Wilkinson et al., Phys. Rev. D 93, 072010 (2016).
- [20] D. Rein and L. M. Sehgal, Ann. Phys. (N.Y.) 133, 79 (1981).
- [21] K. M. Graczyk and J. T. Sobczyk, Phys. Rev. D 77, 053001 (2008).
- [22] K. S. Kuzmin et al., Acta Phys. Pol. B 37, 2337 (2006).
- [23] C. Wilkinson et al., Phys. Rev. D 90, 112017 (2014).
- [24] M. Glu'ck et al., Eur. Phys. J. C 5, 461 (1998).
- [25] A. Bodek and U. K. Yang, AIP Conf. Proc. 670, 110 (2003).
- [26] A. Bodek and U. Yang, AIP Conf. Proc. 792, 257 (2005).
- [27] P. Adamson et al. (MINOS Collaboration), Phys. Rev. D 81, 072002 (2010).
- [28] D. Rein and L. M. Sehgal, Nucl. Phys. B223, 29 (1983).
- [29] D. Rein and L. Sehgal, Phys. Lett. B 657, 207 (2007).
- [30] A. Higuera et al. (MINERvA Collaboration), Phys. Rev. Lett. 113, 261802 (2014).
- [31] T. Sjöstrand, Comput. Phys. Commun. 82, 74 (1994).
- [19] Z. Koba et al., Nucl. Phys. B40, 317 (1972).
- [20] T. Yang et al., Eur. Phys. J. C 63, 1 (2009).
- [21] L. Salcedo et al., Nucl. Phys. A484, 557 (1988).
- [22] D. Ashery et al., Phys. Rev. C 23, 2173 (1981).
- [23] S. G. Mashnik et al., J. Phys. Conf. Ser. 41, 340 (2006).
- [24] K. Abe et al. (T2K Collaboration), Phys. Rev. D 91, 072010 (2015).
- [25] K. Abe et al. (T2K Collaboration), Phys. Rev. D 93, 112012 (2016).
- [26] K. Abe et al., "T2k publicdata," <http://t2k-experiment.org/results>.